Utilization of Underwater Particle Velocity Channels for Data Transmission: Signals, Channels and System Performance

Chen, Chen
Electrical and Computer Engineering Dept.
New Jersey Institute of Technology
Newark, NJ, USA
cc224@njit.edu

Abdi, Ali
Electrical and Computer Engineering Dept.,
New Jersey Institute of Technology
Newark, NJ, USA
ali.abdi@njit.edu

***Abstract*— Recent studies have shown that a vector sensor can serve as a multichannel receiver in underwater communication systems. Here we propose a method to transmit data via the recently introduced underwater particle velocity channels, using a vector dipole sensor. System and channel equations are derived, and system performance results are presented. The results show the possibility of data transmission using a vector sensor in these new channels.**

Keywords-Underwater Communication; Particle Velocity Channels; Dipole Vector Sensors

I. INTRODUCTION

Vector sensors measure the signal not only in the underwater acoustic pressure channel, but also in underwater acoustic particle velocity channels. In [1] a multichannel system is proposed with one pressure sensor as the transmitter and a vector sensor as the receiver. Statistical characteristics of acoustic particle velocity communication channels are discussed in [2]. The focus of this paper is on data transmission using a vector sensor. A dipole vector sensor is composed of two closely-spaced pressure sensors [3]. It is also known that the spatial gradient of acoustic pressure is acoustic particle velocity [3]. This motivates signal modulation on a dipole vector sensor. The spatial gradient between the data on the two pressure sensors of a dipole can be viewed as a signal which is modulated on the dipole, in the direction of axis of the dipole. This means signal transmission via a particle velocity channel. Here, a system with one dipole at the transmitter and a vector sensor at the receiver is proposed. System and channel equations are derived, signal propagation and possible channel correlations in the system are investigated, and finally system performance results are presented.

II. SIGNALS AND CHANNELS IN THE PROPOSED SYSTEM

In the two-dimensional *y*-*z* (range-depth) plane, a vector sensor device measures three components of the field: acoustic pressure, and *y* and *z* components of the acoustic particle velocity. A pressure sensor in the device measures the acoustic pressure. The *y* and *z* components of particle velocity can be measured by two dipoles in *y* and *z* directions, respectively, by spatial differentiation of the acoustic field in each direction. In Fig. 1 there is one dipole at the transmitter and two dipoles at the receiver. The dipole at the transmitter *Tx* is parallel to the *z* axis and the two pressure sensors in *Tx* are labeled as 1 and 2. At the receiver *Rx*, the two dipoles are parallel to *y* and *z* axes with their centers at the point (y_0, z_0). They measure the *y* and *z* components of the acoustic particle velocity at (y_0, z_0). The four pressure sensors at *Rx* are labeled as 1, 2, 3 and 4. Another pressure sensor labeled as 5 is located at (y_0, z_0), to measure the acoustic pressure component in the vector sensor device. So, there are ten different pressure channels in Fig.1, where p_{iq} stands for the channel from sensor *i* at *Tx* to sensor *q* at *Rx*, $i = 1,2$ and $q = 1,2,3,4,5$.

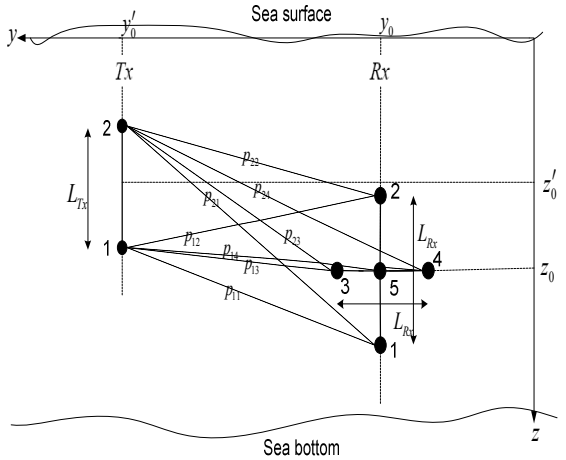

Figure 1. The proposed vector sensor underwater acoustic communication system. There is one transmit dipole and two receive dipoles.

A. System Equations

According to the linearized equation for time-harmonic waves [3], at frequency f_0, for each sensor in *Tx*, there are two particle velocity channels at *Rx*, the vertical and horizontal components of particle velocity at (y_0, z_0). More specifically,

This work is supported in part by the National Science Foundation (NSF), Grant CCF-0830190

for Tx_1 there are $v_z^{Tx_1}$ and $v_y^{Tx_1}$, whereas for Tx_2 we have $v_z^{Tx_2}$ and $v_y^{Tx_2}$. These four channels are given by the following equations, where $L_{Rx} \to 0$

$$\begin{aligned} v_z^{Tx_1} &= -(j\rho_0\omega_0)^{-1}(p_{11}-p_{12})/L_{Rx}, \\ v_z^{Tx_2} &= -(j\rho_0\omega_0)^{-1}(p_{21}-p_{22})/L_{Rx}, \\ v_y^{Tx_1} &= -(j\rho_0\omega_0)^{-1}(p_{13}-p_{14})/L_{Rx}, \\ v_y^{Tx_2} &= -(j\rho_0\omega_0)^{-1}(p_{23}-p_{24})/L_{Rx}. \end{aligned} \quad (1)$$

Here ρ_0 is the density of the fluid, $j^2=-1$, $\omega_0 = 2\pi f_0$ and L_{Rx} denotes the spacing between the two pressure sensors in each dipole at *Rx*, as shown in Fig. 1. To transmit the symbol s, we modulate $s/(jkL_{Tx})$ and $-s/(jkL_{Tx})$ on Tx_1 and Tx_2, respectively, where L_{Tx} denotes the distance between the two sensors in the dipole at *Tx* and $k = 2\pi/\lambda$ is the wavenumber, with λ as the wavelength. Since z velocity is the spatial gradient of the pressure field in the z direction, this transmission scheme means that the symbol s is modulated on the z velocity channel. This can be better understood by writing the equation for the received signal of each pressure sensor at *Rx* as (2). Here $\oplus$ is the convolution. Each channel $(p_{1q}-p_{2q})/(jkL_{Tx})$ in (2), $q=1,2,3,4,5$, is similar to a velocity channel with which the symbol s is convolved. The role of the term jk is clarified in the second paragraph below.

$$\begin{aligned} &r_1 = ((p_{11}-p_{21})/(jkL_{Tx}))\oplus s,\ r_2 = ((p_{12}-p_{22})/(jkL_{Tx}))\oplus s, \\ &r_3 = ((p_{13}-p_{23})/(jkL_{Tx}))\oplus s,\ r_4 = ((p_{14}-p_{24})/(jkL_{Tx}))\oplus s, \\ &r = ((p_{15}-p_{25})/(jkL_{Tx}))\oplus s. \end{aligned} \quad (2)$$

The z and y particle velocity signals at *Rx* are spatial gradients of the received signals r_1, r_2, r_3 and r_4, measured by the two dipoles, as $L_{Rx} \to 0$

$$\begin{aligned} \eta_z &= -(j\rho_0\omega_0)^{-1}(r_1-r_2)/L_{Rx}, \\ \eta_y &= -(j\rho_0\omega_0)^{-1}(r_3-r_4)/L_{Rx}. \end{aligned} \quad (3)$$

By combining (1), (2) and (3), the z and y velocity components at *Rx* can be written as

$$\begin{aligned} \eta_z &= ((v_z^{Tx_1}-v_z^{Tx_2})/(jkL_{Tx}))\oplus s, \\ \eta_y &= ((v_y^{Tx_1}-v_y^{Tx_2})/(jkL_{Tx}))\oplus s. \end{aligned} \quad (4)$$

Now we convert velocity channels and signals to *pressure-equivalent* quantities. Corresponding to the four particle velocity channels in (1), there are four pressure-equivalent particle velocity channels $p_z^{Tx_1}$, $p_z^{Tx_2}$, $p_y^{Tx_1}$, $p_y^{Tx_2}$, obtained by multiplying (1) with the negative of the acoustic impedance $-\rho_0 c$ [1] and using the fact that $\omega_0 = ck$, with c as the sound speed

$$\begin{aligned} p_z^{Tx_1} &= -\rho_0 c v_z^{Tx_1} = (jk)^{-1}(p_{11}-p_{12})/L_{Rx}, \\ p_z^{Tx_2} &= -\rho_0 c v_z^{Tx_2} = (jk)^{-1}(p_{21}-p_{22})/L_{Rx}, \\ p_y^{Tx_1} &= -\rho_0 c v_y^{Tx_1} = (jk)^{-1}(p_{13}-p_{14})/L_{Rx}, \\ p_y^{Tx_2} &= -\rho_0 c v_y^{Tx_2} = (jk)^{-1}(p_{23}-p_{24})/L_{Rx}. \end{aligned} \quad (5)$$

In the above equations we have $L_{Rx} \to 0$. Similarly, the pressure-equivalent z and y velocity components at *Rx* are η_z and η_y multiplied by $-\rho_0 c$

$$r_z = -\rho_0 c\eta_z,\ r_y = -\rho_0 c\eta_y. \quad (6)$$

By substituting (4) into (6) and upon using the definitions in (5) we obtain

$$\begin{aligned} r_z &= ((p_z^{Tx_1}-p_z^{Tx_2})/(jkL_{Tx}))\oplus s, \\ r_y &= ((p_y^{Tx_1}-p_y^{Tx_2})/(jkL_{Tx}))\oplus s. \end{aligned} \quad (7)$$

To include the effect of noise, pressure-equivalent ambient velocity noise terms n_z and n_y should be added to (7), whereas the ambient pressure noise n needs to be added to the last equation in (2). The final set of noisy signals received at *Rx* is given by

$$r = \tilde{p}_d \oplus s + n,\ r_y = \tilde{p}_d^y \oplus s + n_y,\ r_z = \tilde{p}_d^z \oplus s + n_z, \quad (8)$$

where $\tilde{p}_d = (jk)^{-1}(p_{15}-p_{25})/L_{Tx}$, $\tilde{p}_d^y = (jk)^{-1}(p_y^{Tx_1}-p_y^{Tx_2})/L_{Tx}$ and $\tilde{p}_d^z = (jk)^{-1}(p_z^{Tx_1}-p_z^{Tx_2})/L_{Tx}$ are pressure-equivalent impulse responses of the three channels in the system. Note that subscript d indicates that the transmitter is a dipole. Possible correlations among these three channels are studied in Appendix A and B.

B. Channel and Noise Powers

1) Channel Powers

Let $h(\tau)$ be a channel impulse response, with $H(f)$ as its Fourier transform. According to the properties of Bello functions [4] [5], the power of this channel is $\Omega = \int_{-\infty}^{\infty} E[|h(\tau)|^2]d\tau = E[|H(f)|^2]$. The powers of the three channels in (8) are then given by $\Omega_d = \int_{-\infty}^{\infty} E[|\tilde{p}_d(\tau)|^2]d\tau = E[|\tilde{P}_d(f)|^2]$, $\Omega_d^y = \int_{-\infty}^{\infty} E[|\tilde{p}_d^y(\tau)|^2]d\tau = E[|\tilde{P}_d^y(f)|^2]$ and $\Omega_d^z = \int_{-\infty}^{\infty} E[|\tilde{p}_d^z(\tau)|^2]d\tau = E[|\tilde{P}_d^z(f)|^2]$. As shown in Appendix A and B, we have $\Omega_d = \Omega_d^y + \Omega_d^z$.

2) Noise Powers

As shown in [1], for the isotropic noise model, the noise terms in (8) are uncorrelated, that is, $E[nn_y^*] = E[nn_z^*] = E[n_z n_y^*] = 0$. Moreover, for the powers of the noise terms in (8) we have $\Omega_n = E[|n|^2]$ and $\Omega_n^y = E[|n_y|^2] = \Omega_n^z = E[|n_z|^2] = \Omega_n/2$ [1].

III. System Performance and Simulation Results

Let $\tilde{\mathbf{p}}_d = [\tilde{p}_d(0) \ldots \tilde{p}_d(M-1)]^T$, $\tilde{\mathbf{p}}_d^y = [\tilde{p}_d^y(0) \ldots \tilde{p}_d^y(M-1)]^T$ and $\tilde{\mathbf{p}}_d^z = [\tilde{p}_d^z(0) \ldots \tilde{p}_d^z(M-1)]^T$, with ^{T} as transpose, be the taps of the three channel impulse responses in (8). The transmitted symbol vector is defined as $\mathbf{S} = [s_0\ s_1\ s_2\ \cdots\ s_{K-1}]^T$. The channel matrix is $\mathbf{H} = [\mathbf{H}_1^\dagger\ \mathbf{H}_2^\dagger\ \mathbf{H}_3^\dagger]^\dagger$, where † denotes the complex conjugate transpose of a matrix and

$$\mathbf{H}_l = \begin{pmatrix} h_l(0) & & \\ \vdots & \ddots & h_l(0) \\ h_l(M-1) & \ddots & \vdots \\ & & h_l(M-1) \end{pmatrix},\ l = 1,\ 2,\ 3, \quad (9)$$

where $h_1 = \tilde{p}_d$, $h_2 = \tilde{p}_d^y$ and $h_3 = \tilde{p}_d^z$. Let the noise vector be $\mathbf{N} = [\mathbf{N}_1^T\ \mathbf{N}_2^T\ \mathbf{N}_3^T]^T$, where

$$\mathbf{N}_l = [n_l(0)\ n_l(1)\ \cdots\ n_l(K+M-2)]^T,\ l = 1,\ 2,\ 3, \quad (10)$$

and $n_1 = n$, $n_2 = n_y$ and $n_3 = n_z$. These are the noise terms in (8). The vector of received symbols can be written as

$$\mathbf{R} = \mathbf{HS} + \mathbf{N}. \quad (11)$$

Here $\mathbf{R} = [r(0) \cdots r(K+M-2)\ r_y(0) \cdots r_y(K+M-2)\ r_z(0) \cdots r_z(K+M-2)]^T$ and r, r_y and r_z are the received pressure, *y*-velocity and *z*-velocity signals in (8).

Assuming perfect channel estimate at *Rx*, here we use a zero forcing equalizer to investigate the feasibility of symbol detection in the proposed system in Fig. 1. The minimum variance unbiased estimate of the transmitted symbol vector $\mathbf{S}$ is [6]

$$\hat{\mathbf{S}} = (\mathbf{H}^{\dagger}\boldsymbol{\Sigma}^{-1}\mathbf{H})^{-1}\mathbf{H}^{\dagger}\boldsymbol{\Sigma}^{-1}\mathbf{R}, \tag{12}$$

where $\boldsymbol{\Sigma} = E[\mathbf{N}\mathbf{N}^{\dagger}]$ is the covariance matrix of the noise in (11). The covariance matrix of the symbol estimation error can be written as [6]

$$\mathbf{W} = E[(\hat{\mathbf{S}} - \mathbf{S})(\hat{\mathbf{S}} - \mathbf{S})^{\dagger}] = (\mathbf{H}^{\dagger}\boldsymbol{\Sigma}^{-1}\mathbf{H})^{-1}. \tag{13}$$

For binary phase shift keying (BPSK) modulation and similarly to [7] and [8], the average bit error rate (BER) for a block of size *K*, after the zero forcing equalization in (12) can be written as

$$\overline{P}_e = \frac{1}{K}\sum_{i=1}^{K} Q(\sqrt{2\Omega_s / w_{ii}}). \tag{14}$$

Here $\Omega_s = E[|s|^2] = 1$ is the average symbol power with E as the expectation operator, w_{ii} is the *i*-th diagonal element of $\mathbf{W}$ in (13), and $Q(x) = (2\pi)^{-1/2}\int_x^{+\infty}\exp(-x^2/2)dx$.

To define the average signal-to-noise ratio (SNR) per channel in simulations, we first define SNRs in the three channels of the system as $\zeta_d = \Omega_d / \Omega_n$, $\zeta_d^y = \Omega_d^y / \Omega_n^y$, $\zeta_d^z = \Omega_d^z / \Omega_n^z$, where $\Omega_d = (\tilde{\mathbf{p}}_d)^{\dagger}\tilde{\mathbf{p}}_d$, $\Omega_d^y = (\tilde{\mathbf{p}}_d^y)^{\dagger}\tilde{\mathbf{p}}_d^y$ and $\Omega_d^z = (\tilde{\mathbf{p}}_d^z)^{\dagger}\tilde{\mathbf{p}}_d^z$. So, the average SNR per channel is $\overline{\zeta}_d = (\zeta_d + \zeta_d^y + \zeta_d^z)/3$.

The BER of the proposed system is plotted in Fig. 2 using Eq. (14) for the two channels discussed in Appendix A and B. Here we choose $L_{Rx} = L_{Tx} = 0.225\lambda$ such that $E[2|s|^2/(k^2 L_{Tx}^2)] = 1$, which means the average transmit power is 1. Performance of the developed system in [1] with a scalar sensor transmitter and a vector sensor receiver is also given in Fig. 2 as a reference. In the shallow water channel described in Appendix A, our proposed system has nearly 3 dB performance gain over the scalar sensor transmitter system. For the shallow water channel of Appendix B, the two systems have nearly the same BER. The key advantage of the proposed system with a dipole transmitter is that in the reverse (reception) mode, it provides diversity. This is because it can measure both pressure and particle velocity signals.

Now we extend our proposed scheme by modulating one symbol, s_1, on the *z* velocity channel and another symbol, s_2, on the pressure channel. This is accomplished by transmitting $s_1/(jkL_{Tx}) + s_2$ and $-s_1/(jkL_{Tx})$ from Tx_1 and Tx_2 in Fig.1, respectively. With s_1 and s_2 as i.i.d. BPSK symbols and using Alamouti's space-time block code [9], performance of this novel system is shown in Fig. 3 for the two shallow water channels developed in Appendix A and B. For comparison, the performance of a system that uses only the pressure channel at the transmit side is shown in Fig. 3 (BPSK s_1 and s_2 symbols are transmitted from Tx_1 and Tx_2 in Fig.1, respectively, using Alamouti's code). The results show that in both channel types, the proposed system utilizing a particle velocity channel, the *z* velocity channel at transmit side has better BER performance. This further demonstrates the feasibility and usefulness of data modulation in particle velocity channels.

IV. Conclusion

In this paper, data transmission in particle velocity channels for underwater systems is proposed and investigated in detail. Based on the derived system equations and simulation/analytical results, the possibility and performance gain of signal modulation in particle velocity channels is demonstrated. The results provide new opportunities in underwater communication systems.

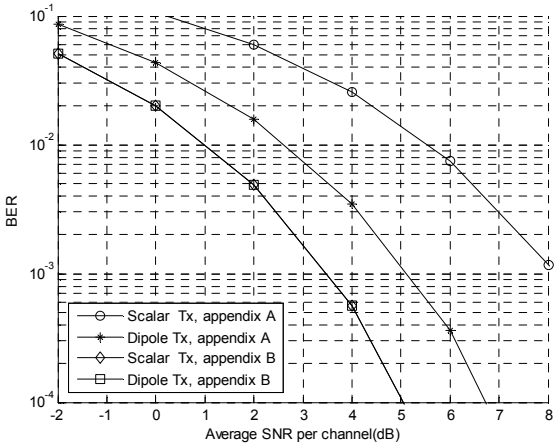

Figure 2. Performance of the proposed system with one transmit dipole and a receive vector sensor, compared to a system with one transmit scalar sensor and a receive vector sensor. Channel parameters of Appendix A are $z_0' = 25$ m, $z_0 = 63$ m, $D_0 = 81.158$ m, $D_y = 1000$ m, $|\beta| = 0.3162$ and $\alpha = 0.01$. Channel parameters of Appendix B are $L_{Tx} = L_{Rx} = 0.225\lambda$, $\sigma_B = \sigma_S = \sigma_b = \sigma_s = \pi/120\ (1.5^\circ)$, $\mu_B = 17\pi/18\ (170^\circ)$, $\mu_S = 192\pi/180\ (192^\circ)$, $\mu_b = \pi/18\ (10^\circ)$, $\mu_s = 348\pi/180\ (348^\circ)$ and $\Lambda_B = \Lambda_b = 0.4$.

Appendix A
A Geometrical Multipath Channel Model

This model is suitable for shallow waters with smooth boundaries, where reflection from the bottom and surface is the dominant propagation mechanism. According to the first bounce after leaving the transmitter and the last bounce before arriving the receiver, rays can be separated into four groups [10][11], they are: first bounce at surface, last bounce at bottom (SB), first bounce at bottom, last bounce at bottom (BB), first bounce at surface, last bounce at surface (SS), and first bounce at bottom, last bounce at surface (BS), in the range-depth plane. When the Rayleigh parameter is much less than unity, boundaries act like reflectors with coherent specular reflection [12], where each received ray can be represented by a direct path from an image of the transmitting source, located outside the channel, towards the receiver [10] [11]. Let the water depth be a constant value D_0 and D_y be the transmission range, such that $D_y \gg D_0$. For a ray from a

transmitter, *Tx*, at (y_0', z_0') to a receiver, *Rx*, at (y_0, z_0), the path length is $\ell_{XW,n} = \sqrt{D_y^{\,2} + A_{XW,n}^2}$ [10] [11], with $A_{XW,n}$ as the vertical distance between the image of *Tx* to *Rx* for the *n*-th ray from the *XW* group, where $X, W = S$ or B. The combined pressure loss is due to multiple surface and bottom reflections [11], where β is the complex surface pressure reflection coefficient and the bottom reflection coefficient is considered to be unity [11]. For each path from *Tx* to *Rx*, the angle of departure (AOD) θ, is measured with respect to the positive *y* axis, counterclockwise. N_{XW} denotes the number of rays in each group. After some mathematical manipulation, the average power in the acoustic pressure and particle *y* and *z* velocity channels are given by (15)-(17). Inspection of (15)-(17) reveals that $\Omega_d = \Omega_d^z + \Omega_d^y$.

$$\begin{aligned}\Omega_d &= E[|\tilde{P}_d(f)|^2] = \sin^2(\theta_0)\cos^2(\theta_0)/D_y^2 \\ &+ \sum_{n_1=1}^{N_{SB}} |\beta|^{2n_1} \sin^2(\theta_{SB,n_1})\cos^2(\theta_{SB,n_1})/D_y^2 \\ &+ \sum_{n_2=1}^{N_{BB}} |\beta|^{2(n_2-1)} \sin^2(\theta_{BB,n_2})\cos^2(\theta_{BB,n_2})/D_y^2 \\ &+ \sum_{n_3=1}^{N_{SS}} |\beta|^{2n_3} \sin^2(\theta_{SS,n_3})\cos^2(\theta_{SS,n_3})/D_y^2 \\ &+ \sum_{n_4=1}^{N_{BS}} |\beta|^{2n_4} \sin^2(\theta_{BS,n_4})\cos^2(\theta_{BS,n_4})/D_y^2, \end{aligned} \tag{15}$$

$$\begin{aligned}\Omega_d^z &= E[|\tilde{P}_d^z(f)|^2] = \sin^4(\theta_0)\cos^2(\theta_0)/D_y^2 \\ &+ \sum_{n_1=1}^{N_{SB}} |\beta|^{2n_1} \sin^4(\theta_{SB,n_1})\cos^2(\theta_{SB,n_1})/D_y^2 \\ &+ \sum_{n_2=1}^{N_{BB}} |\beta|^{2(n_2-1)} \sin^4(\theta_{BB,n_2})\cos^2(\theta_{BB,n_2})/D_y^2 \\ &+ \sum_{n_3=1}^{N_{SS}} |\beta|^{2n_3} \sin^4(\theta_{SS,n_3})\cos^2(\theta_{SS,n_3})/D_y^2 \\ &+ \sum_{n_4=1}^{N_{BS}} |\beta|^{2n_4} \sin^4(\theta_{BS,n_4})\cos^2(\theta_{BS,n_4})/D_y^2, \end{aligned} \tag{16}$$

$$\begin{aligned}\Omega_d^y &= E[|\tilde{P}_d^y(f)|^2] = \sin^2(\theta_0)\cos^4(\theta_0)/D_y^2 \\ &+ \sum_{n_1=1}^{N_{SB}} |\beta|^{2n_1} \sin^2(\theta_{SB,n_1})\cos^4(\theta_{SB,n_1})/D_y^2 \\ &+ \sum_{n_2=1}^{N_{BB}} |\beta|^{2(n_2-1)} \sin^2(\theta_{BB,n_2})\cos^4(\theta_{BB,n_2})/D_y^2 \\ &+ \sum_{n_3=1}^{N_{SS}} |\beta|^{2n_3} \sin^2(\theta_{SS,n_3})\cos^4(\theta_{SS,n_3})/D_y^2 \\ &+ \sum_{n_4=1}^{N_{BS}} |\beta|^{2n_4} \sin^2(\theta_{BS,n_4})\cos^4(\theta_{BS,n_4})/D_y^2. \end{aligned} \tag{17}$$

Similarly to the previous discussion, average correlations between $\tilde{P}_d(f)$, $\tilde{P}_d^z(f)$ and $\tilde{P}_d^y(f)$ can be written as (18)-(20), where they are defined as $\rho_d^z = E[\tilde{P}_d(f)\{\tilde{P}_d^z(f)\}^*]$, $\rho_d^{zy} = E[\tilde{P}_d^z(f)\{\tilde{P}_d^y(f)\}^*]$ and $\rho_d^y = E[\tilde{P}_d(f)\{\tilde{P}_d^y(f)\}^*]$. As a numerical example, magnitudes of (18)-(20), normalized by $\sqrt{\Omega_d \Omega_d^z}$, $\sqrt{\Omega_d^z \Omega_d^y}$ and $\sqrt{\Omega_d \Omega_d^y}$, respectively, are 0.24, 0.24 and 1. The parameters are $D_0 = 81.158$ m, $D_y = 1000$ m, $z_0' = 25$ m, $z_0 = 63$ m, $L_{Tx} = L_{Rx} = 0.2\lambda$, $\alpha = 0.01$ and $|\beta| = 0.3162$, chosen according to [11] with the carrier frequency $f_0 = 12$ kHz. The same correlation magnitudes are observed with $L_{Tx} = L_{Rx} = 0.1\lambda$ and $L_{Tx} = L_{Rx} = 0.5\lambda$.

$$\begin{aligned}\rho_d^z &= E[\tilde{P}_d(f)\{\tilde{P}_d^z(f)\}^*] = -\sin^3(\theta_0)\cos^2(\theta_0)/D_y^2 \\ &- \sum_{n_1=1}^{N_{SB}} |\beta|^{2n_1} \sin^3(\theta_{SB,n_1})\cos^2(\theta_{SB,n_1})/D_y^2 \\ &+ \sum_{n_2=1}^{N_{BB}} |\beta|^{2(n_2-1)} \sin^3(\theta_{BB,n_2})\cos^2(\theta_{BB,n_2})/D_y^2 \\ &+ \sum_{n_3=1}^{N_{SS}} |\beta|^{2n_3} \sin^3(\theta_{SS,n_3})\cos^2(\theta_{SS,n_3})/D_y^2 \\ &- \sum_{n_4=1}^{N_{BS}} |\beta|^{2n_4} \sin^3(\theta_{BS,n_4})\cos^2(\theta_{BS,n_4})/D_y^2, \end{aligned} \tag{18}$$

$$\begin{aligned}\rho_d^{zy} &= E[\tilde{P}_d^z(f)\{\tilde{P}_d^y(f)\}^*] = \sin^3(\theta_0)\cos^3(\theta_0)/D_y^2 \\ &+ \sum_{n_1=1}^{N_{SB}} |\beta|^{2n_1} \sin^3(\theta_{SB,n_1})\cos^3(\theta_{SB,n_1})/D_y^2 \\ &- \sum_{n_2=1}^{N_{BB}} |\beta|^{2(n_2-1)} \sin^3(\theta_{BB,n_2})\cos^3(\theta_{BB,n_2})/D_y^2 \\ &- \sum_{n_3=1}^{N_{SS}} |\beta|^{2n_3} \sin^3(\theta_{SS,n_3})\cos^3(\theta_{SS,n_3})/D_y^2 \\ &+ \sum_{n_4=1}^{N_{BS}} |\beta|^{2n_4} \sin^3(\theta_{BS,n_4})\cos^3(\theta_{BS,n_4})/D_y^2, \end{aligned} \tag{19}$$

$$\begin{aligned}\rho_d^y &= E[\tilde{P}_d(f)\{\tilde{P}_d^y(f)\}^*] = -\sin^2(\theta_0)\cos^3(\theta_0)/D_y^2 \\ &- \sum_{n_1=1}^{N_{SB}} |\beta|^{2n_1} \sin^2(\theta_{SB,n_1})\cos^3(\theta_{SB,n_1})/D_y^2 \\ &- \sum_{n_2=1}^{N_{BB}} |\beta|^{2(n_2-1)} \sin^2(\theta_{BB,n_2})\cos^3(\theta_{BB,n_2})/D_y^2 \\ &- \sum_{n_3=1}^{N_{SS}} |\beta|^{2n_3} \sin^2(\theta_{SS,n_3})\cos^3(\theta_{SS,n_3})/D_y^2 \\ &- \sum_{n_4=1}^{N_{BS}} |\beta|^{2n_4} \sin^2(\theta_{BS,n_4})\cos^3(\theta_{BS,n_4})/D_y^2. \end{aligned} \tag{20}$$

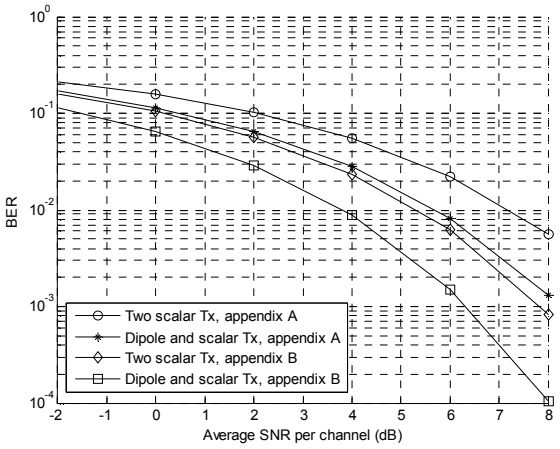

Figure 3. Performance of the proposed system with one dipole and one scalar sensor at the transmit side and a vector sensor at receive side, compared to a system with two scalar sensors at the transmit side and a vector sensor at receive side. Channel parameters are the same as Fig. 2.

APPENDIX B
A STATISTICAL MULTIPATH CHANNEL MODEL

This model is appropriate for shallow water channels with random rough boundaries, where scattering is the dominant mechanism and precise deterministic modeling is not feasible.

Let the transmitter-receiver distance be large enough compared to the channel depth. Consider there is one transmit sensor, Tx_1, and one receive sensor, Rx_1. Denote the double-directional channel transfer function [13] [14] in frequency domain from Tx_1 to Rx_1 as $P_{11}(f)$. Similarly, consider another transmit sensor, Tx_2, and another receive sensor, Rx_2, and denote the double-directional channel transfer function in frequency domain from Tx_2 to Rx_2 as $P_{22}(f)$. By definition, spatial correlation of $P_{11}(f)$ and $P_{22}(f)$ is $C_P(L_{Tx,z}, L_{Tx,y}, L_{Rx,z}, L_{Rx,y}) = E[P_{11}(f)P_{22}^*(f)]$. Using the results of [2], the correlation in this double-directional channel can be written as (21). Here $u_B(\theta^B)$ and $u_S(\theta^S)$ are the probability density functions (PDFs) of the AODs impinging the sea bottom and surface, respectively, $w_b(\gamma^b)$ and $w_s(\gamma^s)$ are the PDFs of the angle of arrivals (AOAs) coming from the sea bottom and surface, respectively. AODs and AOAs are denoted by θ and γ, respectively, both measured with respect to the positive y axis, counterclockwise. The parameters $0 \le \Lambda_b \le 1$ and $1-\Lambda_b$ show what proportions of received rays are finally scattered from bottom and surface, respectively, whereas $0 \le \Lambda_B \le 1$ and $1-\Lambda_B$ indicate the proportions of transmitted rays that first hit the bottom and surface, respectively.

$$\begin{aligned} &C_P(L_{Tx,z}, L_{Tx,y}, L_{Rx,z}, L_{Rx,y}) \\ &= (\Lambda_B \int_0^{\pi} u_B(\theta^B) e^{(jk(L_{Tx,z}\sin(\theta^B)+L_{Tx,y}\cos(\theta^B)))} d\theta^B + \\ &(1-\Lambda_B)\int_{\pi}^{2\pi} u_S(\theta^S) e^{(jk(L_{Tx,z}\sin(\theta^S)+L_{Tx,y}\cos(\theta^S)))} d\theta^S) \\ &\times(\Lambda_b \int_0^{\pi} w_b(\gamma^b) e^{(jk(L_{Rx,z}\sin(\gamma^b)+L_{Rx,y}\cos(\gamma^b)))} d\gamma^b + \\ &(1-\Lambda_b)\int_{\pi}^{2\pi} w_s(\gamma^s) e^{(jk(L_{Rx,z}\sin(\gamma^s)+L_{Rx,y}\cos(\gamma^s)))} d\gamma^s). \end{aligned} \quad (21)$$

Based on the channel definition after (8) and as $L_{Tx} \to 0$ we have $\tilde{P}_d(f) = (jk)^{-1}\partial P(f)/\partial L_{Tx}$, where $P(f)$ is the acoustic pressure measured by a scalar receiver, located at the far field of a scalar transmitter. Similarly, we can write $\tilde{P}_d^z(f) = -k^{-2}\partial^2 P(f)/\partial L_{Tx}\partial L_{Rx}$ and $\tilde{P}_d^y(f) = -k^{-2}\partial^2 P(f)/\partial L_{Tx}\partial L_{Rx}$, where ∂L_{Rx} corresponds to derivative at the receive side in z and y directions, respectively. By inserting these channel representations into the definitions of channel powers at beginning of Sec. II.B.1, powers of the three channels $\tilde{P}_d(f)$, $\tilde{P}_d^z(f)$ and $\tilde{P}_d^y(f)$ can be written in terms of the derivatives of C_P, as follows

$$\begin{aligned} \Omega_d &= -k^{-2}\partial^2 C_P / \partial L_{Tx,z}^2 \,|_{L_{Tx,z}=L_{Tx,y}=L_{Rx,z}=L_{Rx,y}=0}, \\ \Omega_d^z &= k^{-4}\partial^4 C_P / \partial L_{Tx,z}^2 \partial L_{Rx,z}^2 \,|_{L_{Tx,z}=L_{Tx,y}=L_{Rx,z}=L_{Rx,y}=0}, \\ \Omega_d^y &= k^{-4}\partial^4 C_P / \partial L_{Tx,z}^2 \partial L_{Rx,y}^2 \,|_{L_{Tx,z}=L_{Tx,y}=L_{Rx,z}=L_{Rx,y}=0}. \end{aligned} \quad (22)$$

Using (21) and (22) it can be shown that $\Omega_d = \Omega_d^z + \Omega_d^y$.

Channel correlations between $\tilde{P}_d(f)$, $\tilde{P}_d^z(f)$ and $\tilde{P}_d^y(f)$, defined as $\rho_d^z = E[\tilde{P}_d(f)\{\tilde{P}_d^z(f)\}^*]$, $\rho_d^{zy} = E[\tilde{P}_d^z(f)\{\tilde{P}_d^y(f)\}^*]$ and $\rho_d^y = E[\tilde{P}_d(f)\{\tilde{P}_d^y(f)\}^*]$, can be similarly calculated using the following relations

$$\begin{aligned} \rho_d^z &= jk^{-3}\partial^3 C_P / \partial L_{Tx,z}^2 \partial L_{Rx,z} \,|_{L_{Tx,z}=L_{Tx,y}=L_{Rx,z}=L_{Rx,y}=0}, \\ \rho_d^{zy} &= k^{-4}\partial^4 C_P / \partial L_{Tx,z}^2 \partial L_{Rx,z} \partial L_{Rx,y} \,|_{L_{Tx,z}=L_{Tx,y}=L_{Rx,z}=L_{Rx,y}=0}, \\ \rho_d^y &= jk^{-3}\partial^3 C_P / \partial L_{Tx,z}^2 \partial L_{Rx,y} \,|_{L_{Tx,z}=L_{Tx,y}=L_{Rx,z}=L_{Rx,y}=0}. \end{aligned} \quad (23)$$

Now we use the Gaussian angular model [2]. More specifically, there are two AOD random variables θ^B and θ^S, hitting the bottom and surface with parameters (μ_B, σ_B) and (μ_S, σ_S), respectively, where μ and σ denote the mean and standard deviation of a Gaussian distribution, respectively. Similarly, there are two AOA random variables γ^b and γ^s received from the bottom and surface, with parameters (μ_b, σ_b) and (μ_s, σ_s), respectively. With parameters $L_{Tx} = L_{Rx} = 0.2\lambda$, $\sigma_B = \sigma_S = \sigma_b = \sigma_s = \pi/120$ (1.5°), $\mu_B = 17\pi/18$ (170°), $\mu_S = 192\pi/180$ (192°), $\mu_b = \pi/18$ (10°), $\mu_s = 348\pi/180$ (348°) and $\Lambda_B = \Lambda_b = 0.4$, magnitudes of normalized channel correlations $\rho_d^z / \sqrt{\Omega_d \Omega_d^z}$, $\rho_d^{zy} / \sqrt{\Omega_d^z \Omega_d^y}$ and $\rho_d^y / \sqrt{\Omega_d \Omega_d^y}$, obtained from (22) and (23) are, respectively, 0.28, 0.27 and 1. A figure not provided here due to space limitations shows that the normalized correlation magnitudes appear to be relatively insensitive to the small angle spreads σ.

REFERENCES

[1] A. Abdi and H. Guo, "A new compact multichannel receiver for underwater wireless communication networks," IEEE Trans. Wireless Commun., vol. 8, pp. 3326-3329, 2009.

[2] A. Abdi and H. Guo, "Signal correlation modeling in acoustic vector sensor arrays," IEEE Trans. Signal Processing, vol. 57, pp. 892-903, 2009.

[3] C. H. Sherman and J. L. Butler, Transducers and Arrays for Underwater Sound, New York: Springer, 2007.

[4] G. D. Durgin, Space-Time Wireless Channels, Upper Saddle River, NJ: Prentice-Hall PTR, 2003.

[5] R. Janaswamy, Radiowave Propagation and Smart Antennas for Wireless Communications, Boston: Kluwer, 2001.

[6] S. M. Kay, Fundamentals of Statistical Signal Processing: Estimation Theory, Englewood Cliffs, NJ: PTR Prentice-Hall, 1993.

[7] S. Ohno, "Performance of single-carrier block transmissions over multipath fading channels with linear equalization," IEEE Trans. Signal Processing, vol. 54, pp. 3678 – 3687, 2006.

[8] C. Tepedelenlioglu and Q. Ma, "On the performance of linear equalizers for block transmission systems," in Proc. IEEE Global Telecommun. Conf., St. Louis, MO, 2005, pp. 3892-3896.

[9] N. Al-Dhahir, "Single-carrier frequency-domain equalization for space-time block coded transmissions over frequency-selective fading channels," IEEE Commun. Lett., vol.5, pp. 304-306, 2001.

[10] L. M. Brekhovskikh and Yu. P. Lysanov, Fundamentals of Ocean Acoustics, New York: Springer, 2003.

[11] A. Zielinski, Y. H. Yoon and L. Wu, "Performance analysis of digital acoustic communication in a shallow water channel," J. Oceanic Eng. , vol. 20, pp. 293-299, 1995.

[12] R. J. Urick, Principles of Underwater Sound, New York: McGraw-Hill, 1975.

[13] H. Xu, D. Chizhik, H. Huang and R. Valenzuela, "A generalized space-time multiple-input multiple-output (MIMO) channel model," IEEE Trans. Wireless Commun., vol. 3, pp. 966-975, 2004.

[14] A. F. Molisch, Wireless Communication, New York: Wiley, 2005.